



Study on Residual Stress Releasing of 316L Stainless Steel Welded Joints by Ultrasonic Impact Treatment

Xiaodong Hu¹ · Chongbin Ma¹ · Yicheng Yang¹ · Qingliang Zeng¹

Received: 11 July 2018 / Accepted: 3 April 2020 / Published online: 15 April 2020
© Korean Society of Steel Construction 2020

Abstract

In this paper, the effect of ultrasonic impact treatment (UIT) on the residual stress of 316L welded butt-joint was investigated. Firstly, the temperature field distribution in the welded joint was simulated based on the double-ellipsoidal heat source model, and the residual stresses were calculated by a sequential coupling thermo-mechanical finite element method. Subsequently, based on the theory of transient contact mechanics, the effects of UIT on releasing of the welding residual stress was analyzed. The microstructure of the weld metal before and after the UIT treatment was compared to study the influence of UIT. The results show that the maximum residual stresses in the weld metal and heat affected zones are released due to the dislocation multiplication during the UIT, and this effect on the weld metal is more remarkable than that on the heat affected zones. The results of numerical simulation of UIT are consistent with the corresponding experimental results. After UIT, the transverse and longitudinal tensile stresses near the fusion line are changed to compressive stresses.

Keywords Welded joint · Residual stress · Microstructure analysis · Ultrasonic impact treatment · Finite element method

1 Introduction

Welding technology has been widely used in the fields of aviation, nuclear, pressure vessels and mechanical manufacturing due to its low cost and desirable mechanical properties (Teng et al. 2001). On the other hand, due to the non-uniform welding temperature distribution and large constraint, complex residual stresses are generated during welding (Wan et al. 2017). Welding residual stress is one of the critical factors affecting the strength of welded products (Jiang et al. 2018). Meanwhile, tensile residual stresses are generally detrimental and have a significant influence on the susceptibility of a weld to fatigue damage, stress corrosion cracking and fracture (Zhang et al. 2017, 2018). Therefore, the release of residual stress is a problem that needs to be solved for the welded structure. Annealing treatment, vibratory stress relief, hammer peening, shot peening, laser shock peening, temperature stretching eliminates stress et al. are the commonly used post-weld treatment techniques (Yuan

and Sumi 2016; Gong et al. 2009). However, the above method is not suitable for large welded parts such as large underwater structures and bridges. Therefore, with the wide application of high-strength steel in large-scale welded structures, it is necessary to find ways to improve or eliminate the residual stress of large high-strength steel welded structures. Ultrasonic impact treatment (UIT) is a remarkable post-weld technique, which has been widely used to improve the stress state at the weld seam of high strength steel with the advantages of low energy consumption, high efficiency, small size, lightweight, flexible use, good controllability and minimal noise (Zammit et al. 2015; Okawa et al. 2013; Yuan and Sumi 2015).

The UIT reduces the local stress concentration by changing the geometry of the weld toe and reduces the tensile residual stress by introducing compressive residual stress (Deng and Murakawa 2006). In recent years, the effect of UIT on the welding residual stress and the fatigue performance of weld joints have been paid much attention in Refs. Liu et al. (2016), Foehrenbach et al. (2016), Dekhtyar et al. (2015). Turски et al. (2010) found that the UIT can produce compressive residual stress fields to 2 mm depth on the 8 mm-thick 304L stainless steel. Cheng et al. (2003) found that a compressive stress layer was not less than 1 mm in depth at the weld toe after UIT. Roy and

✉ Xiaodong Hu
huxdd@163.com

¹ College of Mechanical and Electronic Engineering, Shandong University of Science and Technology, Qingdao 266590, People's Republic of China

Fisher (2005) found that the partial defects in the welded joint disappeared and the surface grain become finer after the UIT (Rai et al. 2014). Moreover, UIT can cause a homogeneous distribution of residual stress with pressure stress formed on the surface of the weld (Statnikov et al. 2013; Roy et al. 2003). The severe plastic deformation on the surface of titanium alloy after UIT was analyzed by Mordyuk (2016) with a two-dimensional finite element method (FEM). Zheng et al. (2018) studied the residual stresses of 304L stainless steel weld joints after UIT by three-dimensional finite element. It was found that the fatigue lives of weld joints can be extended remarkably after the UIT. However, the research work in this field is not perfect at present, especially the combination analysis of the numerical simulation of UIT, the experiment of UIT, the microstructure change of the metal after UIT and the mechanism of eliminating the residual stress of the welding has rarely been studied. If we can understand the relationship between the four sides, it will provide a numerical basis for the study of UIT and the optimization of its manufacturing process for UIT elimination welding residual stress.

In this paper, the welding residual stress distribution of a 316L welded butt-joint was studied by the experimental method and numerical analysis. The effects UIT on releasing of the residual stress of the welded joint were analyzed. The microstructure of the welded specimens was observed to clarify the influence of UIT on the metallographic organization.

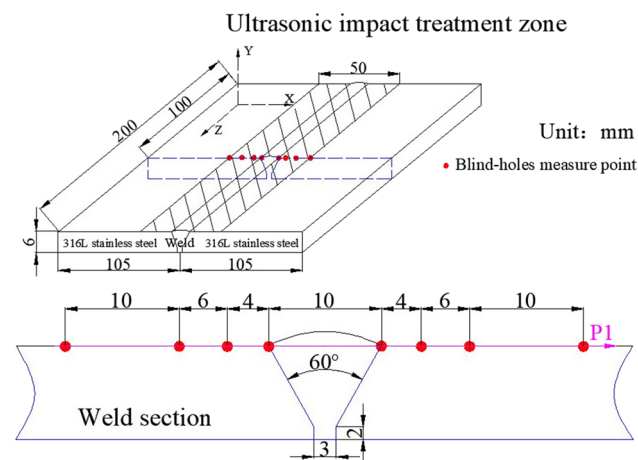


Fig. 1 Schematic of dimensions of the welded joint and the UIT zone

Table 1 Chemical composition (wt%)

Element	C	Cr	Ni	Mo	Si	Mn	P	S
316L	0.020	16.770	12.340	2.290	0.023	1.860	0.027	0.023
ER316L	0.025	19.10	12.58	2.57	0.42	1.91	0.015	0.008

2 Materials and Experimental Procedure

2.1 Welding Test and Microstructure Observation

Figure 1 shows the sketching of the weld sample. Two 316L austenitic stainless steel plates with dimensions of 200×100×6 mm were welded together by using tungsten inert gas (TIG) welding. The material of the Electrode is ER316L with the diameter of 2.5 mm. Their chemical compositions are tested by the Electron Probe Microscope-analyzer (EPMA) and listed in Table 1.

The shielding gas is Ar and the gas flow rate is 13 L/min. The welding current, the welding voltage, and the welding speed are 120 A, 13 V and 8 cm/min, respectively. The weld heat efficiency is 0.89. No incomplete fusion and pore defects were found by radiographic inspection. Optical microscope (OM) was used to analyze the metallographic microstructure of the butt-joint. Electron Probe Microscope-analyzer (EPMA) was used to analyze the energy spectra.

2.2 Residual Stress Measurement

The residual stress in the central area of the upper surface of the welded sample was measured by blind-holes method. Blind-holes with dimensions of Φ1.5×1.5 mm were drilled. The strains in three directions of each blind hole, i.e., in the directions of 0°, 45° and 90° of the blind hole were measured. The residual stress of the initial test point was calculated by Eqs. (1), (2), (3) according to the measured strain value (Bo et al. 2014).

$$\sigma_1 = \frac{E}{4A}(\epsilon_1 + \epsilon_3) - \frac{E}{4B}\sqrt{(\epsilon_1 - \epsilon_3)^2 + (2\epsilon_2 - \epsilon_1 - \epsilon_3)^2} \tag{1}$$

$$\sigma_2 = \frac{E}{4A}(\epsilon_1 + \epsilon_3) + \frac{E}{4B}\sqrt{(\epsilon_1 - \epsilon_3)^2 + (2\epsilon_2 - \epsilon_1 - \epsilon_3)^2} \tag{2}$$

$$\text{tg}2\theta = \frac{2\epsilon_2 - \epsilon_1 - \epsilon_3}{\epsilon_3 - \epsilon_1} \tag{3}$$

where ϵ_1 , ϵ_2 , and ϵ_3 are the measured strain in the direction of 0°, 45° and 90°, respectively. A and B are the release coefficients related to the geometric size of the blind-hole, the size of the strain gauge and the material properties. E is the elasticity modulus of the material. Figure 2 shows the sketching of the measurement of the weld joint by blind-holes measurement.

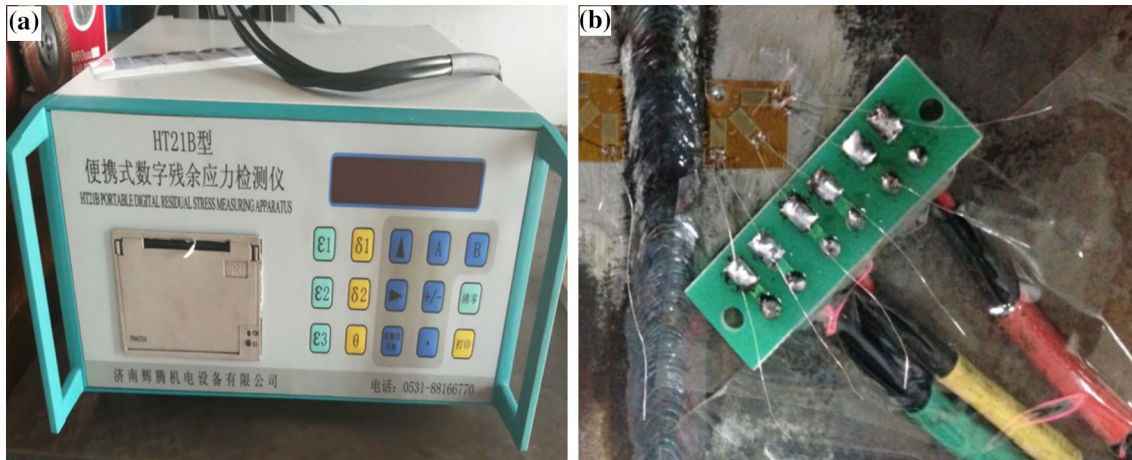


Fig. 2 Sketch of the measurement of the weld joint by blind-holes measurement

Totally 8 blind holes were drilled, the positions of them are shown in Fig. 1. They located on a line perpendicular to the weld. The six holes are located in the base metal, while the other two holes are located a the fusion lines.

2.3 Ultrasonic Impact Treatment

After completing the surface residual stress measurement, the impact pin was impacted on the entire weld surface. It moves along the direction perpendicular to the weld seam. The zone with a width of 50 mm illustrated in Fig. 1 was impacted by the pin head with a diameter of 6 mm. The vibration output amplitude, the ultrasonic frequency the output power are 40 μm , 20 kHz and 450–500 W, respectively. The moving speed of the impact pin is 4 mm/s. The number of reciprocating impacts is two times. Figure 3 shows the sketch of the weld joint by UIT.



Fig. 3 Sketch of the weld joint by UIT

3 Numerical Simulation

3.1 Finite Element Model for Welding

A coupled finite element program (Jiang et al. 2010b) was developed to simulate the temperature field and the residual stress after welding of 316L austenitic stainless steel with finite element software ABAQUS.

(1) Meshing

The refined meshes were created in the vicinity of the weld region and the HAZ to obtain more accurate results. The minimum element size was selected as $0.33 \times 0.33 \times 0.33$ mm in the weld zone. The element types for temperature simulation and residual stress calculation are DC3D8 and C3D8R, respectively. In total,

30,702 nodes and 26,220 elements have meshed. The same meshing is used in the temperature and residual stress simulation.

(2) Material properties

It is assumed that the dependence of thermodynamic properties on temperature is the same for HAZ, the weld metal, and the base metal (Jiang et al. 2016). For thermal and mechanical analyses, temperature-dependent thermo-physical and mechanical properties are incorporated. The temperature dependency of physical and mechanical properties of 316L (Jiang et al. (2012)) are shown in Fig. 4. In addition, the latent heat, the solidus temperature and the liquidus temperature of 316L are 300 kJ/kg, 1420 °C, 1460 °C, respectively.

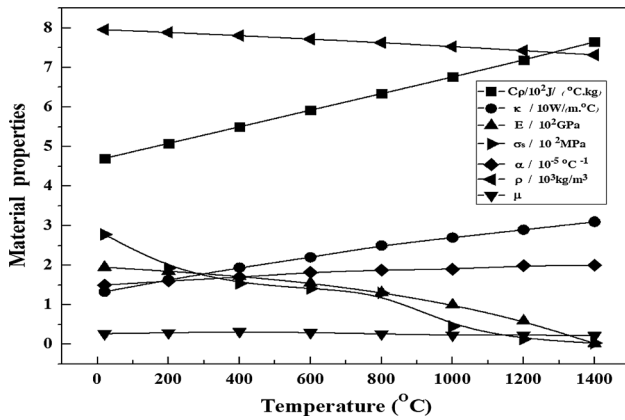


Fig. 4 Thermodynamic properties of 316L (C_p -specific heat, K -thermal conductivity, E -Young’s modulus, σ_s -yield strength, α -thermal expansion, ρ -density, μ -Poisson’s ratio)

(3) Welding temperature analysis

In the thermal analysis, the welding process is primarily simulated by applying a double-ellipsoidal heat source model. The front and rear heat flux distributions of the heat source model can be described by Eqs. (4) and Eq. (5) (Jiang et al. 2017).

For the front heat source is calculated with Eq. (4).

$$q(xyzt) = \frac{6\sqrt{3}f_f Q}{abc_1\pi\sqrt{\pi}} e^{-3x^2/a^2} e^{-3y^2/b^2} e^{-3(z-vt-z_0)^2/c_1^2} \quad (4)$$

For the rear heat source is calculated with Eq. (5).

$$q(xyzt) = \frac{6\sqrt{3}f_r Q}{abc_2\pi\sqrt{\pi}} e^{-3x^2/a^2} e^{-3y^2/b^2} e^{-3(z-vt-z_0)^2/c_2^2} \quad (5)$$

where f_f and f_r give the fractions of the heat deposited in the front and the rear parts, respectively. Note that $f_f + f_r = 2.0$. It assumes that the f_f is 1.6 and f_r is 0.4 considering that the temperature gradient in the front leading part is steeper than that of the trailing edge. Q is the power of the welding heat source and the z_0 is the position of the heat source in z -direction when t is zero. x , y , and z are the local coordinates of the double ellipsoid model aligned with the welded plate. The parameters a , b , c_1 , and c_2 related to the characteristics of the welding arc, are 3, 3, 4, and 8 mm, respectively. The heat source of double ellipsoidal distribution is modeled by a user subroutine DFLUX in ABAQUS with defined movement compiled by FORTRAN program.

In the welding process, the heat exchange between the workpiece and the surrounding air is conducted by con-

vection and radiation (Jiang et al. 2010a). The convective heat exchange between the numerical calculation model and the environment is described by the Newton cooling Eq. (6) (Jiang et al. 2014).

$$q_a = -h_a(T_s - T_a) \quad (6)$$

where q_a is the convective heat exchange between the numerical calculation model and the environment; h_a is convection coefficient ($10 \text{ W/m}^2 \cdot \text{K}$). T_s and T_a are the surface temperature and room temperature (20°C), respectively.

For the heat radiation is calculated with Eq. (7) (Jiang et al. 2014).

$$q_h = -\varepsilon\sigma \left[(T_s + 273.15)^4 - (T_a + 273.15)^4 \right] \quad (7)$$

where ε is emissivity (0.85); σ is Stefan–Boltzmann constant.

(4) Residual stress analysis

The residual stress is calculated by using the temperature distribution obtained from welding temperature analysis as input data. Birth and Death technology is also used in stress analysis. The material properties relevant to residual stress are elastic modulus, yield stress, Poisson’s ratio, and coefficient of thermal expansion. It is assumed that there is no phase transformation, and the total strain rate can be decomposed into three components as Eq. (8) (Xie et al. 2017).

$$\varepsilon = \varepsilon^e + \varepsilon^p + \varepsilon^{ts} \quad (8)$$

where ε^e , ε^p and ε^{ts} stand for elastic strain, plastic strain, and thermal strain, respectively. The elastic strain can be calculated based on isotropic Hooke’s law with temperature-dependent Young’s modulus and Poisson’s ratio. The thermal strain is calculated according to the temperature-dependent coefficient of thermal expansion. For the plastic strain, a rate-independent plastic model is employed with a von Mises yield surface, temperature-dependent mechanical properties, and isotropic hardening model.

3.2 Numerical Model for Ultrasonic Impact Treatment

The procedure of UIT strengthening is a contact problem of highly transient impact dynamics. Explicit dynamic FEM was used to solve the computational model.

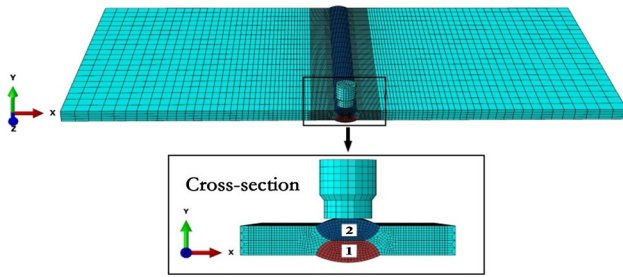


Fig. 5 Finite element model for ultrasonic impact treatment

(1) Ultrasonic impact treatment model

The UIT simulation was performed by importing welding residual stresses as the initiating state. The pin model was set as a rigid body. Because the target hardness is much lower than that of the impact pin. The finite element model for UIT is shown in Fig. 5.

(2) Material constitutive relationship

Dynamic plastic deformation is localized on the surface of 316L stainless steel during the UIT process. The yield limit and yield stress of the material depend on strain rates. Johnson–Cook model was used in this study. The yield limit of 316L is expressed by Eq. (9).

$$\sigma = (A + B\bar{\epsilon}^n)(1 + C \ln \dot{\epsilon}^*)(1 - T^{*m}) \quad (9)$$

where $\bar{\epsilon}$ is the equivalent plastic strain; $\dot{\epsilon}^*$ is the dimensionless plastic strain rate; T^{*m} is the dimensionless temperature term; A is the yield strength; B is work hardening modulus; C is the strain rate sensitivity constant; n is the work hardening coefficient, m is the temperature softening coefficient. The temperature effect caused by the UIT can be neglected because the phase transition temperature of the material is much larger than the test temperature. The Johnson–Cook parameters of 316L are shown in Table 2 (Correa et al. 2015).

(3) Load and boundary conditions

Displacement load was applied on the impact pin (see Fig. 3) along the Z-direction (i.e. the thickness direction of the welding plate). The amplitude of displacement loading, the moving speed of impact pin, the impact width is 0.04 mm, 4 mm/s, 50 mm, respectively. Two reciprocating impacts with sine wave displacement loading with a frequency of 20 kHz were adopted.

Table 2 Johnson–Cook parameters of 316L stainless steel

A (MPa)	B(MPa)	C	n	m	ϵ'_o
300	600	0.045	0.35	0.5	1

4 Results and Discussion

4.1 Microstructure Observation

There are four solidification modes in austenitic stainless steel weld: full Austenite (A), Austenite and Ferrite (AF), Ferrite and Austenite (FA) and full Ferrite (F).

Figure 6 is a pseudo-binary diagram of austenitic stainless steel weld. The equivalents of chromium and nickel in Schaeffler’s tissue diagram can be calculated based on the corresponding equations.

The chromium equivalent can be calculated by Eq. (10).

$$Creq = \%Cr + \%Mo + (1.5 \times \%Si) + (0.5 \times \%Nb) \quad (10)$$

The nickel equivalent can be calculated by Eq. (11).

$$Nieq = \%Ni + (30 \times \%C) + (30 \times \%N) + (0.5 \times \%Mn) \quad (11)$$

The chromium equivalent and nickel equivalent of 316L is 21.81% and 12.88%, respectively. The $Creq/Nieq = 1.69$ corresponds to FA solidification mode in Fig. 6.

FA solidification type is residual lath ferrite in austenite with uneven crystal interface and high fracture toughness. Figure 7a illustrates the Scanning Electron Microscope (SEM) morphology of the weld metal located at the center of the weld seam. It is found that intermittent skeleton ferrite distributes on the columnar austenite matrix, which is the ferrite–austenite solidification structure. It indicates that ferrite is precipitated from the liquid firstly during the solidification process. Then the austenite is produced with

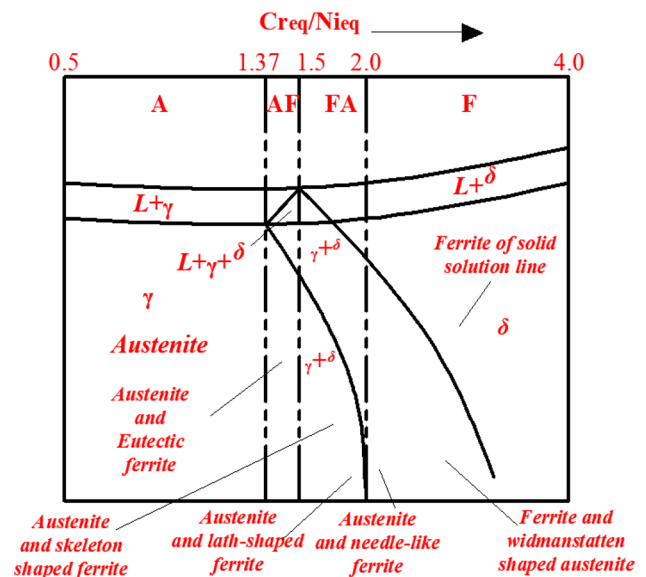


Fig. 6 Diagram of the solidification mode and the pseudo-binary diagram

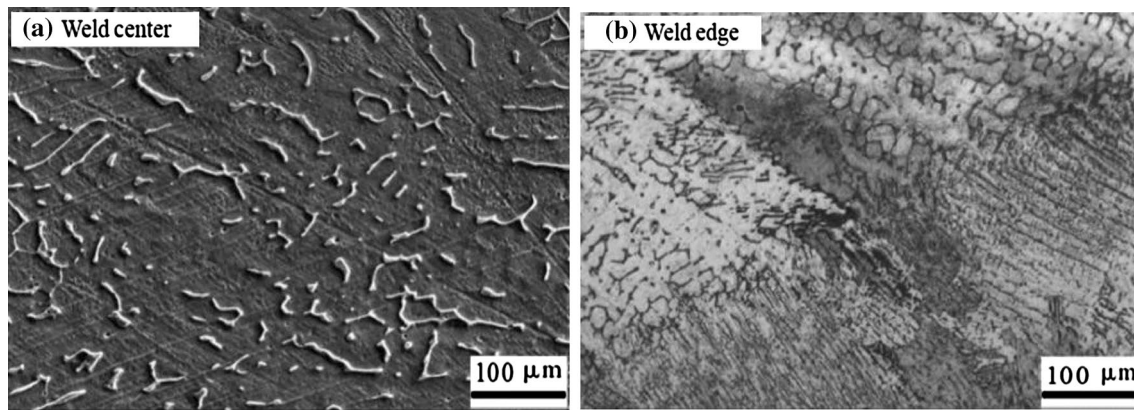


Fig. 7 The microstructure of different regions in the weld

the peritectic transformation. Finally, the structure consists of austenite and retained ferrite surrounded by austenite. The Ferrite distributes uniformly in the austenite matrix and forms uneven grain boundaries, which is beneficial to resist the crack propagation in the weld.

Figure 7b is the OM morphology of the weld metal located at weld seam edge. It is observed that the microstructure consists of a dense row of small columnar dendrites perpendicular to the fusion line. The welding center is a mixture of ferrite and austenite under dense FA solidification mode.

The microstructure and the results of line scanning by EDS of weld center are shown in Fig. 8. The dendritic line is rich in chromium, and the content of C and Cr has a great peak, while the content of Ni decreased obviously. Therefore, it is judged that the ferrite in the weld microstructure solidified by FA mode in the weld, and the ferrite in the weld is distributed on the dendrites axis of rich chromium by vermicular form.

4.2 The Influence of UIT on the Microstructure of the Weld Metal

The microstructures of the butt-joint before and after UIT are shown in Fig. 9. The fusion line before UIT is clearly visible in Fig. 9a. The equiaxed austenite with coarse grains existed in HAZ close to the fusion line. Moreover, there are clear slip lines inside the grain. It can be concluded that significant plastic deformation occurred based on the slip band slip with dense slip line which has a high degree of parallelism. It indicates that large residual stress is produced in HAZ.

After UIT, the fusion line becomes blurred, as shown in Fig. 9b. In this case, refined equiaxed grains arranged densely with uniform distribution. And the grains of the HAZ are larger than that of the weld zone. The grains in the HAZ are difficult to be deformed due to the steady state even though the high frequency and high energy input of UIT.

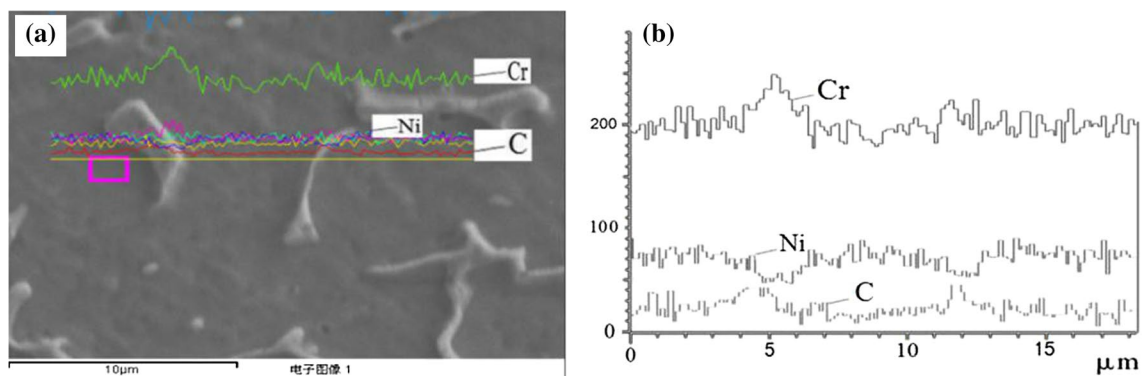


Fig. 8 Microstructure and line scanning map of the weld metal located at the center of the weld seam

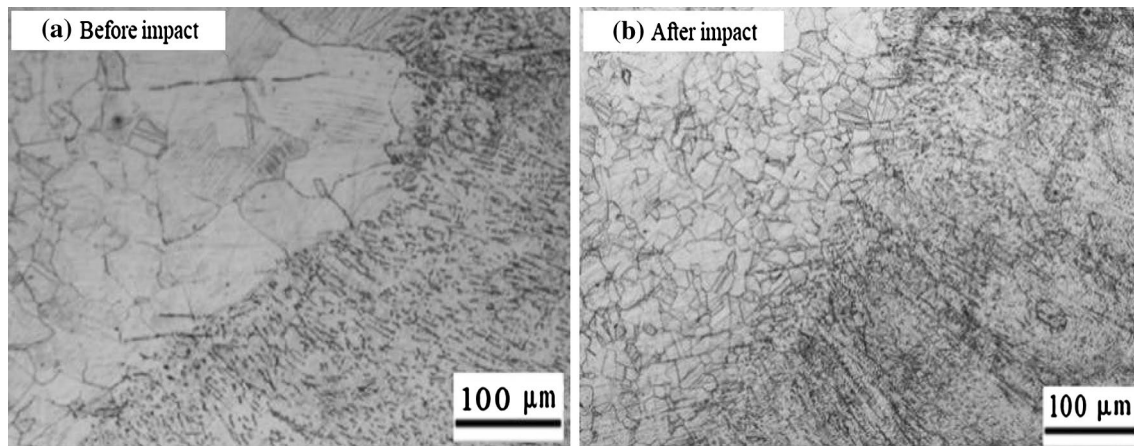


Fig. 9 The microstructure of welded joint before and after ultrasonic impact treatment

4.3 Micro-mechanism Analysis

The high-frequency energy caused by ultrasonic impact was input on the surface of the weld seam. The crystals in it bear the high-frequency vibration. It leads to remarkable surface plastic deformation, distortion of lattice and migration of grain boundary. The two basic types of dislocations in crystals are edge dislocations and screw dislocations. However, the dislocations present in real crystals are generally coexisting mixed dislocations. Figure 10 shows the procedure of formation of the mixed dislocation.

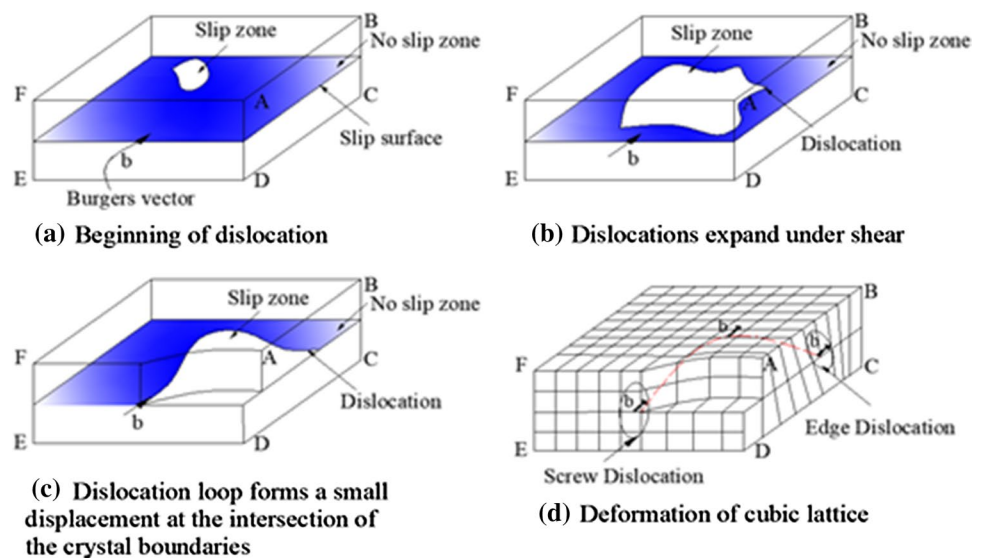
The dislocation of crystal grains slips under shear stress from the position with relatively high energy to a position with relatively low energy. The total dislocation energy decreases and the dislocation density increases greatly. The dislocations become uniform and small, which directly leads to the release of residual stress.

4.4 As-Welded Residual Stress Analysis

The residual stress distribution of the welded joint before and after UIT is shown in Fig. 8. It is found that the transverse residual stress in welding seam and the HAZ region before UIT is relative large (see Fig. 11a). The largest tensile residual stress value is up to 298 MPa. Transverse residual stress distributes symmetrically on both sides of the weld seam. And the residual stress decreases gradually from the weld zone to the base metal zone. After UIT, the transverse residual stress in the weld and HAZ reduced significantly (see Fig. 11b). Transverse residual stress still distributes symmetrically. And the largest tensile residual stress value is 185 MPa.

The longitudinal residual stress in welding seam and the HAZ region before UIT is relative large (see Fig. 12 a). The largest tensile residual stress value is up to 247 MPa. The

Fig. 10 Schematic illustration of mixed dislocation



residual stress is compressed away from the weld zone. And, the compress the residual stress distributes symmetrically on both sides of the weld seam. After UIT, the longitudinal residual stress in the weld and HAZ decreased obviously (see Fig. 12b). The longitudinal residual stress in weld and HAZ is the transition from tensile residual stress to compressive residual stress. Longitudinal residual stress still distributes symmetrically. And the largest tensile residual stress value is 197 Mpa.

The residual stress of thickness of weld interior zone and surface zone of the weld seam before UIT is tensile stress(see Fig. 13a). However, the surface zone of the weld seam is compressive residual stress. After UIT, the residual stress of thickness of weld interior zone and surface zone of the weld seam changes little (see Fig. 13b). And, the residual

stress becomes homogeneous. The overall tensile residual stress increases. The largest tensile residual stress value is 119 MPa.

4.5 Effects of UIT on Weld Residual Stresses

The path marked as P1 in Fig. 1 was chosen to analysis the residual stress distribution before and after the UIT. The residual stress in vertical weld direction (transverse residual stress) and parallel weld direction (longitudinal residual stress) have a great influence on fatigue structure of steel. Therefore, combined with the residual stress test, the transverse residual stress and the longitudinal residual stress were analyzed with the comparison of numerical simulation and experimental results.

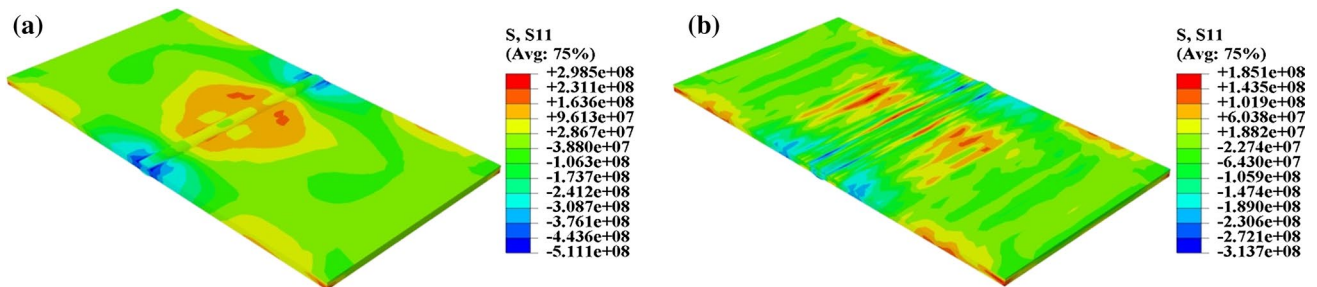


Fig. 11 The contour of transverse residual stress before (a) and after (b) ultrasonic impact treatment

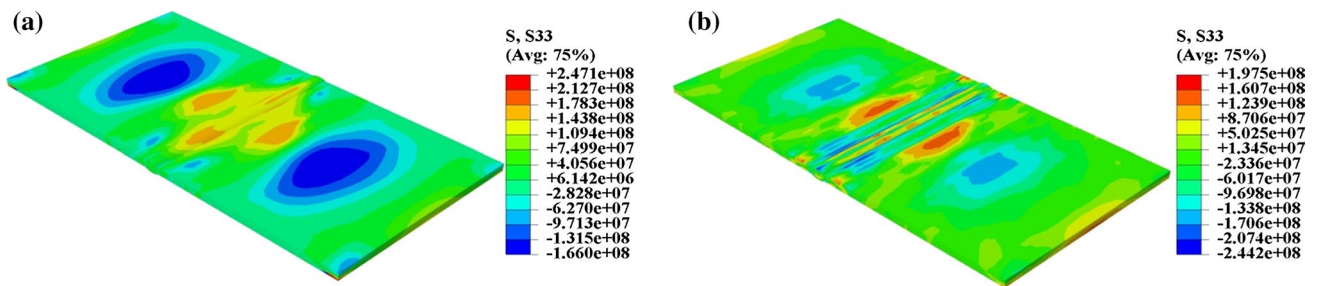


Fig. 12 The contour of longitudinal residual stress before (a) and after (b) ultrasonic impact treatment

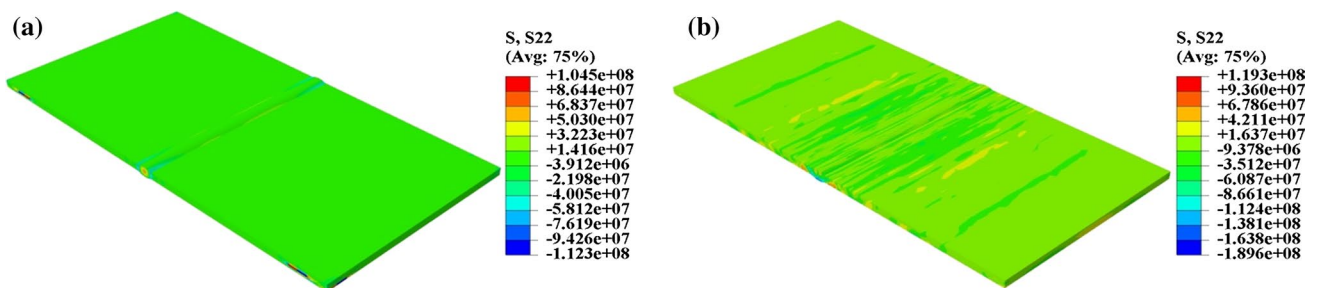


Fig. 13 The contour of thickness residual stress before (a) and after (b) ultrasonic impact treatment

Comparison of the measured and the calculated transverse residual stress and longitudinal residual stress along P1 are shown in Figs. 14 and 15, respectively. It includes both results before and after the UIT. The transverse residual stresses at the eight test points in the weld zone, the HAZ and base metal are tensile stresses. The maximum transverse residual stress in the weld zone is 106.92 MPa, the maximum transverse residual stress in HAZ is 94.45 MPa, and transverse residual stress in the weld zone is 98.7 MPa. After UIT, the transverse residual stress in the weld zone is reduced to 12.51 MPa, which is reduced by 94.41 MPa; the transverse stress residual in HAZ is reduced to 21.08 MPa, which is reduced by 73.37 MPa; the transverse stress residual in base metal is reduced to 26.4 MPa, which is reduced by 72.3 MPa. The maximum longitudinal residual stress in the weld zone is 109 MPa, the maximum longitudinal residual stress in HAZ is 101 MPa, and longitudinal residual stress in the weld zone is 100 MPa. After UIT, the longitudinal residual stress in the weld zone is compressive stress, and value of compressive stress is 95 MPa, which reduced

by 204 MPa; the longitudinal stress residual in HAZ is compressive stress, and value of compressive stress is 15 MPa, which reduced by 116 MPa; the longitudinal stress residual in base metal is compressive stress, and value of compressive stress is 10 MPa, which reduced by 110 MPa. The numerical simulation value of transverse residual stress is basically consistent with the experimental value before and after the UIT simulation. Shimanuki and Okawa (2013) estimated the fatigue life of these cruciform joints by crack growth analysis based on the crack opening and closure simulation using the modified strip-yielding model, accounting for the residual stress distribution created by welding or UIT. These estimation results demonstrate good agreement with experimental results obtained at various stress ratios. Roy and Fisher (2005) used the simplified stress-life method of finite element analysis to estimate the fatigue strength of parts with infinite life after UIT. The results of finite element simulation are consistent with the experimental results.

The stress on both sides of the weld is mainly tensile stress before UIT as shown in Fig. 14, and the residual stress

Fig. 14 The result comparisons of the numerical simulation and the experiment of the transverse residual stress in the path P1 direction before and after UIT

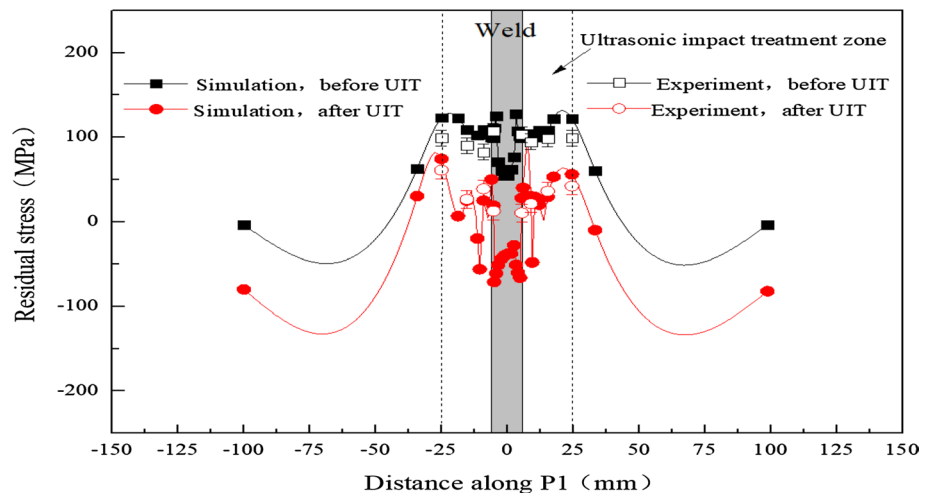


Fig. 15 The result comparisons of the numerical simulation and the experiment of the longitudinal residual stress in the path P1 direction before and after UIT

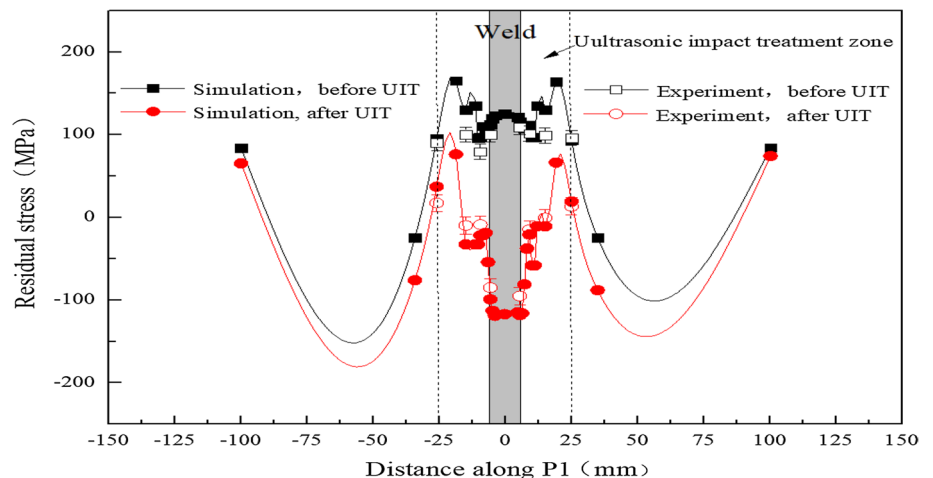
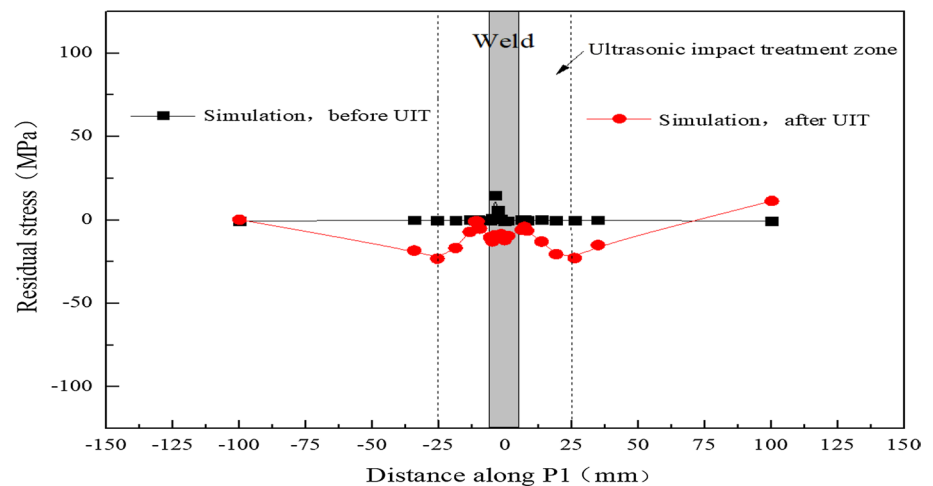


Fig. 16 The residual stress of thickness direction along path P1 direction before and after ultrasonic impact treatment



of middle of the weld surface is the transition from tensile residual stress to compressive residual stress. The transverse residual stress is tensile stress and the main stress in the weld zone. The maximum transverse stress values are around 5 mm of the weld, that is the fusion line on the upper surface of the weld. As the boundary point of solid–liquid in the weld is subjected to strong thermal action and force during welding and cooling, the stress of which is complex with the maximum tensile stress value is 128 MPa. After UIT, the transverse residual stress decreased significantly, and the welding residual tensile stress on the near surface of the plate was converted into numerically unequal residual compressive stress before UIT. In the UIT zone, the transverse residual tensile stress in the weld zone and the HAZ decreases significantly. The residual tensile stress is transformed into a beneficial residual compressive stress, and the amplitude of residual compressive stress is larger. The maximum value of compressive stress is up to 94 MPa at the fusion line. The transverse residual tensile stress also decreases in varying degrees apart from the UIT zone.

The longitudinal residual stress distribution along the path P1 before and after the UIT is shown in Fig. 15. The longitudinal residual stress distribution is similar to the transverse residual stress distribution before UIT, but the trend is different. There is an obvious compressive stress zone far away from the weld. The maximum longitudinal residual stress appears near the the weld and the HAZ with the largest tensile stress value up to 171 MPa. In the welding process, the temperature of the weld is the highest, the temperature of the parent material far away from the weld is low, and the residual stress level is low. The residual stress in the base zone far away from the weld is low because the temperature of which is much lower than the temperature of the weld during the welding process. The stress distribution on both sides of the weld line tends to be symmetrical. After UIT, the longitudinal tensile stress decreases significantly in the UIT zone. The

residual tensile stress in weld zone and HAZ turn to beneficial residual compressive stress. The amplitude of residual compressive stress is large, and the maximum value is up to 125 MPa at the fusion line. The longitudinal residual stress far from the UIT zone decreases little with the UIT. Foehrenbach et al. (2016) developed a computationally efficient approach to predict residual stresses induced by the UIT process using a commercial finite element software package. It was found that compressive residual stresses up to a base material yield strength occurred after the UIT treatment. The implied cold working by the UIT induced plastic deformation of the weld joint. The same level of residual stress exceeding the yield stress of material was also measured by previous researchers (Turcki et al. 2010; Roy et al. 2003). And, the UIT introduced compressive stresses in the upper surface of weld joints, which had a beneficial effect on fatigue strength of material (Yuan and Sumi 2016; Ranjan et al. 2016; Ghahremani et al. 2015; Liu et al. 2014).

The normal residual stress distribution along the thickness direction of P1 before and after UIT is shown in Fig. 16. The overall stress level of the thickness residual stress is relatively low before UIT, and there is no obvious change. After UIT, the residual stress of thickness direction of the UIT zone was decreased. The welding residual compressive stress is converted to smaller residual tensile stress the zone far from UIT zone.

5 Conclusions

This paper presents a study of residual stress distribution before and after the UIT in welding joint 316L stainless steel by FEM and measurement, and the effect of microstructure of the weld metal before and after the UIT has been discussed. The obtained conclusions are as following:

1. The 316L weld metal consists of austenite and ferrite, and the ferrite is mainly distributed in dendrites principal axis in the shape of a worm. The microstructure in the fusion line is a vertical columnar dendrite. The grains in the HAZ grow obviously, and there is an obvious slip band on the surface.
2. The numerical simulation results of UIT are in good agreement with the experimental values, which proves that it is feasible to calculate the welding residual stresses by numerical simulation of UIT.
3. The transverse and longitudinal residual stresses in the welded joint before and after the UIT are all symmetrical with respect to the weld center. Before UIT, the transverse residual stress of the joint is mainly tensile stress, and the maximum value was found at the weld line. The maximum longitudinal residual stress appears near the weld and HAZ. The transverse residual tensile stress of the joints is converted to residual compressive stress after UIT. The maximum longitudinal residual compressive stress occurs near the weld and HAZ.
4. After UIT, the transverse residual stress in the weld zone, HAZ and base metal are reduced by 94.41 MPa, 73.37 MPa, and 72.3 MPa, respectively. After UIT, the longitudinal residual stress in the weld zone, HAZ and base metal are reduced by 204 MPa, 116 MPa, and 110 MPa, respectively.
5. The residual stresses in the weld metal and HAZ of welded joints are significantly reduced by the UIT. This is due to the input of high-frequency energy of ultrasonic impact, leads to the decrease of total dislocation energy, then results in the increase of dislocation density. Finally, the dislocations becoming uniform and small leads to the release of residual stress.

Acknowledgements The authors gratefully acknowledge the support provided by the Nature Science Foundation of Shandong Province (2018GGX103019).

References

- Bo, L., Kaihui, H., Dongwei, S., Weicai, Y., & Jun, S. (2014). Research on measurement of residual stresses of hemispherical lithium hydride by blind-hole method. *Fusion Engineering and Design*, 89(4), 365–369.
- Cheng, X., Fisher, J. W., Prask, H. J., Gnäupel-Herold, T., Yen, B. T., & Roy, S. (2003). Residual stress modification by post-weld treatment and its beneficial effect on fatigue strength of welded structures. *International Journal of Fatigue*, 25(9), 1259–1269.
- Correa, C., Lara, L. R. D., Díaz, M., Gil-Santos, A., Porro, J. A., & Ocaña, J. L. (2015). Effect of advancing direction on fatigue life of 316L stainless steel specimens treated by double-sided laser shock peening. *International Journal of Fatigue*, 79, 1–9.
- Dekhtyar, A. I., Mordiyuk, B. N., Savvakina, D. G., Bondarchuk, V. I., Moiseeva, I. V., & Khripta, N. I. (2015). Enhanced fatigue behavior of powder metallurgy Ti–6Al–4V alloy by applying ultrasonic impact treatment. *Materials Science and Engineering: A*, 641, 348–359.
- Deng, D., & Murakawa, H. (2006). Numerical simulation of temperature field and residual stress in multi-pass welds in stainless steel pipe and comparison with experimental measurements. *Computational Materials Science*, 37(3), 269–277.
- Foehrenbach, J., Hardenacke, V., & Farajian, M. (2016). High frequency mechanical impact treatment (HFMI) for the fatigue improvement: Numerical and experimental investigations to describe the condition in the surface layer. *Welding in the World*, 60(4), 1–7.
- Ghahremani, K., Ranjan, R., Walbridge, S., & Ince, A. (2015). Fatigue strength improvement of aluminum and high strength structures using high frequency mechanical impact treatment. *Procedia Engineering*, 133, 465–476.
- Gong, J., Jiang, W., Fan, Q., Chen, H., & Tu, S. T. (2009). Finite element modelling of brazed residual stress and its influence factor analysis for stainless steel plate-fin structure. *Journal of Materials Processing Technology*, 209(4), 1635–1643.
- Jiang, W., Chen, W., Woo, W., Tu, S. T., Zhang, X. C., & Em, V. (2018). Effects of low-temperature transformation and transformation-induced plasticity on weld residual stresses: Numerical study and neutron diffraction measurement. *Materials & Design*, 147, 65–79.
- Jiang, W., Fan, Q., & Gong, J. (2010a). Optimization of welding joint between tower and bottom flange based on residual stress considerations in a wind turbine. *Energy*, 35(1), 461–467.
- Jiang, W., Liu, Z., Gong, J. M., & Tu, S. T. (2010b). Numerical simulation to study the effect of repair width on residual stresses of a stainless steel clad plate. *International Journal of Pressure Vessels & Piping*, 87(8), 457–463.
- Jiang, W., Luo, Y., Li, J. H., & Woo, W. (2017). Residual stress distribution in a dissimilar weld joint by experimental and simulation study. *Journal of Pressure Vessel Technology*, 139(1), 011402.
- Jiang, W., Luo, Y., Wang, B. Y., Tu, S. T., & Gong, J. M. (2014). Residual stress reduction in the penetration nozzle weld joint by overlay welding. *Materials & Design*, 60(8), 443–450.
- Jiang, W., Zhang, Y., & Woo, W. (2012). Using heat sink technology to decrease residual stress in 316L stainless steel welding joint: finite element simulation. *International Journal of Pressure Vessels & Piping*, 92(4), 56–62.
- Jiang, W., Zhang, Y. C., Zhang, W. Y., Luo, Y., Woo, W., & Tu, S. T. (2016). Growth and residual stresses in the bonded compliant seal of planar solid oxide fuel cell: Thickness design of window frame. *Materials & Design*, 93, 53–62.
- Liu, C., Ge, Q., Chen, D., Gao, F., & Zou, J. (2016). Residual stress variation in a thick welded joint after ultrasonic impact treatment. *Science & Technology of Welding & Joining*, 21(8), 624–631.
- Liu, Y., Wang, D., Deng, C., Xia, L., Huo, L., & Wang, L. (2014). Influence of re-ultrasonic impact treatment on fatigue behaviors of S690QL welded joints. *International Journal of Fatigue*, 66, 155–160.
- Mordiyuk, B. N., Prokopenko, G. I., Grinkevich, K. E., Piskun, N. A., & Popova, T. V. (2016). Effects of ultrasonic impact treatment combined with the electric discharge surface alloying by molybdenum on the surface related properties of low-carbon steel G21Mn5. *Surface & Coatings Technology*, 328, 344–354.
- Okawa, T., Shimanuki, H., Funatsu, Y., Nose, T., & Sumi, Y. (2013). Effect of preload and stress ratio on fatigue strength of welded joints improved by ultrasonic impact treatment. *Welding in the World*, 57(2), 235–241.
- Rai, P. K., Pandey, V., Chattopadhyay, K., Singhal, L. K., & Singh, V. (2014). Effect of ultrasonic shot peening on microstructure and mechanical properties of high-nitrogen austenitic stainless

- steel. *Journal of Materials Engineering & Performance*, 23(11), 4055–4064.
- Ranjan, R., Ghahremani, K., Walbridge, S., & Ince, A. (2016). Testing and fracture mechanics analysis of strength effects on the fatigue behavior of hfmi-treated welds. *Welding in the World*, 60(5), 1–13.
- Roy, S., & Fisher, J. W. (2005). Enhancing fatigue strength by ultrasonic impact treatment. *International Journal of Steel Structures*, 5(3), 241–252.
- Roy, S., Fisher, J. W., & Yen, B. T. (2003). Fatigue resistance of welded details enhanced by ultrasonic impact treatment (UIT). *International Journal of Fatigue*, 25(9), 1239–1247.
- Shimanuki, H., & Okawa, T. (2013). Effect of stress ratio on the enhancement of fatigue strength in high performance steel welded joints by ultrasonic impact treatment. *International Journal of Steel Structures*, 13(1), 155–161.
- Statnikov, E. S., Muktepavel, V. O., & Blomqvist, A. (2013). Comparison of ultrasonic impact treatment (UIT) and other fatigue life improvement methods. *Welding in the World*, 46(3–4), 20–32.
- Teng, T. L., Fung, C. P., Chang, P. H., & Yang, W. C. (2001). Analysis of residual stresses and distortions in t-joint fillet welds. *International Journal of Pressure Vessels & Piping*, 78(8), 523–538.
- Turski, M., Clitheroe, S., Evans, A. D., Rodopoulos, C., Hughes, D. J., & Withers, P. J. (2010). Engineering the residual stress state and microstructure of stainless steel with mechanical surface treatments. *Applied Physics A*, 99(3), 549–556.
- Wan, Y., Jiang, W., Li, J., Sun, G., Kim, D. K., & Woo, W. (2017). Weld residual stresses in a thick plate considering back chipping: Neutron diffraction, contour method and finite element simulation study. *Materials Science & Engineering A*. <https://doi.org/10.1590/1980-5373-MR-2017-0926>.
- Xie, X. F., Jiang, W., Luo, Y., Xu, S., Gong, J. M., & Tu, S. T. (2017). A model to predict the relaxation of weld residual stress by cyclic load: Experimental and finite element modeling. *International Journal of Fatigue*, 95, 293–301.
- Yuan, K., & Sumi, Y. (2016). Simulation of residual stress and fatigue strength of welded joints under the effects of ultrasonic impact treatment (UIT). *International Journal of Fatigue*, 92, 321–332.
- Yuan, K. L., & Sumi, Y. (2015). Modelling of ultrasonic impact treatment (UIT) of welded joints and its effect on fatigue strength. *Frattura Ed Integrità Strutturale*, 6(34), 476–486.
- Zammit, U., Marinelli, M., Pizzoferrato, R., & Mercuri, F. (2015). A review of ultrasonic peening treatment. *Materials & Design*, 87(12), 1072–1086.
- Zhang, W., Jiang, W., Zhao, X., & Tu, S. T. (2018). Fatigue life of a dissimilar welded joint considering the weld residual stress: Experimental and finite element simulation. *International Journal of Fatigue*, 109, 23.
- Zhang, Y. C., Jiang, W., Tu, S. T., Zhang, X. C., Ye, Y. J., & Zhang, Y. C. (2017). Creep crack growth behavior analysis of the 9cr-1mo steel by a modified creep-damage model. *Materials Science & Engineering A*, 708, 68–76.
- Zheng, J., Ince, A., & Tang, L. (2018). Modeling and simulation of weld residual stresses and ultrasonic impact treatment of welded joints. *Procedia Engineering*, 213, 36–47.

Publisher's Note Springer Nature remains neutral with regard to jurisdictional claims in published maps and institutional affiliations.